CHINESE OPTICS LETTERS

Vol. 20, No. 2 | February 2022

PbS quantum dots and BaF_2:Tm^{3+} nanocrystals co-doped glass for ultra-broadband near-infrared emission [Invited]

Wei Wang (王 伟)[1], Qinpeng Chen (陈钦鹏)[1], Yifei Zhao (赵逸飞)[2], Yakun Le (乐亚坤)[1], Shengda Ye (叶昇达)[1], Mang Wan (万 芒)[3], Xiongjian Huang (黄雄健)[1,4*], and Guoping Dong (董国平)[1**]

[1] State Key Laboratory of Luminescent Materials and Devices, Guangdong Provincial Key Laboratory of Fiber Laser Materials and Applied Techniques, Guangdong Engineering Technology Research and Development Center of Special Optical Fiber Materials and Devices, School of Materials Science and Engineering, South China University of Technology, Guangzhou 510640, China

[2] Department of Chemistry, City University of Hong Kong, Kowloon 999077, Hong Kong, China

[3] Analytical and Testing Center, South China University of Technology, Guangzhou 510640, China

[4] School of Physics and Optoelectronics, South China University of Technology, Guangzhou 510640, China

*Corresponding author: hxj@scut.edu.cn

**Corresponding author: dgp@scut.edu.cn

Received September 30, 2021 | Accepted November 10, 2021 | Posted Online December 9, 2021

With the rapid growth of optical communications traffic, the demand for broadband optical amplifiers continues to increase. It is necessary to develop a gain medium that covers more optical communication bands. We precipitated PbS quantum dots (QDs) and BaF_2 : Tm^{3+} nanocrystals (NCs) in the same glass to form two independent emission centers. The BaF_2 NCs in the glass can provide a crystal field environment with low phonon energy for rare earth (RE) ions and prevent the energy transfer between RE ions and PbS QDs. By adjusting the heat treatment schedule, the emission of the two luminescence centers from PbS QDs and Tm^{3+} ions perfectly splices and covers the ultra-broadband near-infrared emission from 1200 nm to 2000 nm with bandwidth over 430 nm. Therefore, it is expected to be a promising broadband gain medium for fiber amplifiers.

Keywords: PbS quantum dot; Tm^{3+}; nanocrystal-glass composite; broadband near-infrared emission.
DOI: 10.3788/COL202220.021603

1. Introduction

With the advent of the big data age, the application of broadband fiber amplifiers has become more and more important[1–4]. Replacing repeaters with simple, low cost, and broadband fiber amplifiers to increase the non-relay distance has become a continuous research topic in the current optical fiber communication field. At present, rare earth (RE) ion-doped fiber amplifiers are relatively mature in laser devices, such as Er^{3+}[5], Ho^{3+}[6], Tm^{3+}[7], Yb^{3+}[8], and Nd^{3+}[9] ions and their combinations[10–12]. Due to the extranuclear electron orbit characteristics of RE ions, the emission of RE ions originates from the $4f$–$4f$ transition, which results in a fixed emission wavelength with a narrow bandwidth[13]. Although the emission of RE ions can be enhanced and broadened by adding a sensitizer, their doping concentrations are usually no more than 2% to avoid the loss of excitation energy caused by cross relaxation[14]. The emission bandwidths of transition metal (TM) ions can reach several hundreds of nanometers due to their d–d orbital transitions, which is a better choice for realizing broadband luminescence. However, the luminescence of TM ions is very sensitive to the environment, and the glass network with a weak crystal field leads to low luminescence efficiency of TM ions[15–17].

In recent years, semiconductor quantum dot (QD)-doped glasses with tunable wavelength and broadband emission have attracted much attention[18–21]. Semiconductor QDs with different bandgaps, such as PbS QDs and PbSe QDs, are obtained by nucleation and crystal-growth mechanisms in different glass matrices under thermal field treatment. In our previous work, we have studied the influence of the introduction of the PbS QDs precursor on the luminescence spectra of QD-doped glass and detected the optical amplification signals at 1330 nm and 1530 nm in the samples[22]. Furthermore, we have successfully fabricated all-solid-state PbS QD-doped glass fibers with tunable near-infrared (NIR) emission by using the melt-in-tube method[23]. However, the emission range (1000–1700 nm) and the bandwidths of PbS QDs-doped glass cannot be further expanded, which limits the properties of optical amplification.

RE ions and semiconductor QDs are both efficient luminescent materials. Whether the effective combination of them can produce high-efficiency luminescence or laser devices has always been a question to researchers. Meijerink *et al.*[24] reported the successful coupling of CdSe QDs with the Yb^{3+} ions. The adsorption of Yb^{3+} on the surface of CdSe QDs showed energy transfer from the QD to the $^2F_{5/2}$ state of Yb^{3+}, creating an emission in the NIR regions. Serqueira *et al.*[25] confirmed a quantitative description of the cross section of energy transfer between Nd^{3+} ions and QDs through the rate equations model. Nd^{3+} ions were embedded in a glass system with CdS QDs, which can increase the quantum efficiency of Nd^{3+} ions. Recently, our group added Tm^{3+} ions in the CdS QD-doped glass and obtained white-light emission through energy transfer between Tm^{3+} ions and CdS QDs[26]. Although these works have proved that RE ions can be incorporated into QDs, energy transfer occurs between them, which makes it impossible to effectively broaden the emission band.

In this work, Tm^{3+}-ion- doped BaF_2 nanocrystals (NCs) and PbS QDs were simultaneously precipitated in the glass through post thermal treatment. Different from previous work[24–26], BaF_2 NCs can provide a crystal field with lower phonon energy, which enhances the emission intensity of Tm^{3+} ions and avoids energy transfer between Tm^{3+} ions and PbS QDs. Therefore, ultra-broadband NIR emission covering 1200–2000 nm with a full width at half-maximum (FWHM) over 430 nm was obtained by combining the emission from PbS QDs and BaF_2 : Tm^{3+} NCs under the excitation of an 808 nm laser diode (LD).

2. Experiments

2.1. Fabrication

The glasses were prepared by the melt-quenching method with a composition of $15SiO_2$-$40B_2O_3$-10ZnO-$22K_2O$-$13BaF_2$-1PbO-1ZnS-$3TmF_3$ (mole fraction). After being fully mixed, 30 g stoichiometric raw materials were melted at 1100°C for 30 min in a low-temperature furnace. The glass melt was quenched on a preheated stainless-steel plate to form transparent glasses and then transferred to the muffle furnace at 350°C for 3 h to eliminate the inner stress. After the glasses were completely cooled, the precursor glasses (PGs) without QDs and NCs were obtained, then cut into suitable sizes (1 cm × 1 cm), and underent heat treatment at 460°C–480°C for 10 h. Afterward, PbS QDs and BaF_2 NCs were formed in the glasses.

2.2. Characterization

The glasses were analyzed by X-ray diffraction (XRD, PANalytical X′pert PRO, Cu Kα, $\lambda = 1.540598$ Å) to determine the crystal forms in the glass. Transmission electron microscopy (TEM, Tecnai G2, FEI, Amsterdam, the Netherlands) was used to confirm the size, size distribution, and morphology of PbS QDs and BaF_2 NCs. A UV/visible (VIS)/NIR double beam spectrophotometer (Perkin-Elmer Lambda 900, Waltham, MA) was used to measure the absorption spectra of the glasses. An Omni k300 spectrometer (Zolix, China) was utilized to record the fluorescence spectra upon the excitation of an 808 nm LD. The lifetime decay curves of the glass samples were measured by a digital phosphor oscilloscope (TDS3012C, Tektronix, America) and a signal generator. The variable temperature spectrum test was also measured by the Omni k300 spectrometer (Zolix, China) for testing. Orient-KOJI's TAP-02 high-temperature fluorescence accessory was used as an external device for the spectrometer, and the test range was from room temperature to 453 K.

2.3. Calculation

Theoretical simulations were carried out based on the density functional theory (DFT) and the generalized gradient approximation (GGA) Perdew–Burke–Ernzerhof (PBE) exchange-correlation functional for describing the interactions[27,28]. The plane wave cutoff energy was set to be 400 eV. A $3 \times 3 \times 3$ k-mesh centered at the gamma point was used for all calculations. All of the structures were allowed to relax until the energy on the atoms was less than 5.0×10^{-4} eV, and all of the forces on atoms are below 0.2 eV/Å.

3. Results

Figure 1(a) shows the differential scanning calorimetry (DSC) curve of the PG. According to the curve, the glass transition temperature (T_g) of the PG is 402°C and the exothermic peak at 473.7°C is the crystallization peak (T_p) of the PG. Thus, the heat treatment temperature range is set to 460°C–480°C. Figure 1(b) is the XRD pattern of the PG and the glass is heat treated at different temperatures for 10 h. There are only amorphous peaks in the XRD curves of the PG, indicating that there are no crystals in

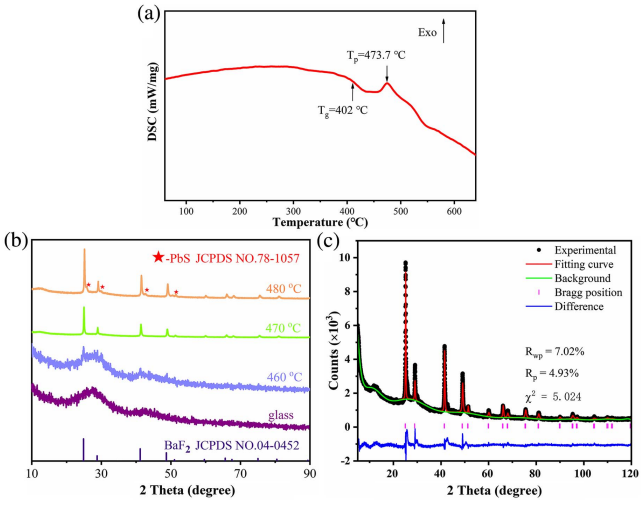

Fig. 1. (a) DSC curves of PG. (b) XRD patterns of PG and glasses heat treated at different temperatures for 10 h. (c) XRD refinement patterns of glass heat treated at 480°C for 10 h.

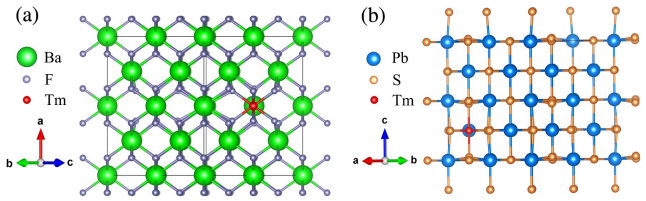

Fig. 2. Crystal structure of (a) BaF_2 and (b) PbS doped with a Tm^{3+} ion.

the PG. As the heat treatment temperature increases, sharper diffraction peaks appear at 470°C, and the intensity of the diffraction peaks becomes stronger. The three weak diffraction peaks appearing at 26°, 30°, and 43° in the sample heat treated at 480°C refer to the (111), (200), and (220) crystal planes of the cubic structure of PbS QDs. The other three diffraction peaks appearing at 25°, 29°, and 41° in the sample are ascribed to the (111), (200), and (220) crystal planes of BaF_2 NCs, respectively. According to the Scherrer formula calculation, the average particle size of BaF_2 NCs in the samples heat treated at 470°C and 480°C is about 33.41 nm and 38.59 nm, respectively. It can be observed that the diffraction peaks of BaF_2 NCs heat treated at 480°C shifted to larger angles compared to the standard card. This indicates that Tm^{3+} ions entered the BaF_2 NCs lattice, resulting in the change of the unit cell parameters. Through refinement of the XRD curve, as shown in Fig. 1(c), it is found that the volume of the crystal ($a = 6.17726$) is reduced compared with that of the standard crystal ($a = 6.2001$).

To find out why Tm^{3+} ions tend to enter the BaF_2 NCs instead of PbS QDs, theoretical simulations were then employed to investigate the defect formation energies of Tm^{3+} ions in BaF_2 or PbS (Fig. 2). A $2 \times 2 \times 2$ supercell was built based on the pristine lattice of PbS (Fm-3m) and BaF_2 (Fm-3m) before one Tm^{3+} atom was introduced. The structures were fully relaxed under the same criterion, and the defect formation energy was then calculated by the following equation:

$$E^f(\text{defect}) = E_{\text{tot}}(\text{defect}) - E_{\text{tot}}(\text{perfect}) - \sum_i n_i \mu_i, \quad (1)$$

where E_{tot}(defect) and E_{tot}(perfect) are the total energy of the cells with and without defects. $\sum_i n_i \mu_i$ is the change in chemical potential before and after introducing the defects, in which μ_i is the corresponding chemical potential of the elements, and n_i is the number of atoms. μ_{Pb}, μ_{Ba}, and μ_{Tm} were correspondingly derived from Pb (Fm-3m), Ba (Im-3m), and Tm ($P6_3/mmc$). The calculated results were listed in Table 1. The Tm-Ba incorporation is the most likely to take place since it has a smaller formation energy (0.91 eV), while Tm^{3+} ions are difficult to be introduced into the PbS lattice due to the higher formation energy of 7.03 eV. The simulation results reveal that the Tm^{3+} ions preferentially enter the BaF_2 lattice during the formation of NCs.

To further confirm the formation and morphology of crystals in the designed glass samples, the microstructure and element distribution of the glass heat treated at 470°C were studied by

Table 1. Key Parameters for the Defect Formation Energy Calculation.

Model	Total Energy (eV)	$\sum_i n_i \mu_i$ (eV)	Formation energy (eV)
Perfect BaF_2	−549.23	0	0
BaF_2:Tm	−550.59	−2.26	0.91
Perfect PbS	−269.93	0	0
PbS:Tm	−263.98	−1.08	7.03

TEM measurement, as shown in Fig. 3. It can be seen that two NCs with different sizes are precipitated in the glass sample under 470°C heat treatment, namely 3–4 nm and 32–35 nm, corresponding to the sizes of PbS QDs and BaF_2 NCs in XRD. The high-resolution TEM (HRTEM) image shows that the lattice fringe of the larger crystal is 0.31 nm, which corresponds to the (200) crystal plane of BaF_2 NCs [Fig. 3(b)], and the lattice fringe of the other crystal is 0.21 nm, which corresponds to the (220) crystal plane of PbS QDs [Fig. 3(c)]. To further analyze the distribution of PbS QDs, BaF_2 NCs, and Tm^{3+} ions in the glass, a two-dimensional elemental mapping analysis was performed on the sample. Due to the smaller size of PbS QDs, only BaF_2 NCs are observed in the strong diffraction region [Fig. 3(d)]. In the strong diffraction region, it can be observed that Ba, F, and Tm elements are more abundantly distributed in the NC region than in the glass phase, which indicates that Tm^{3+} ions are concentrated around BaF_2 NCs in the glass [Figs. 3(g)–3(i)].

Figure 4 shows the absorption spectra of the PG and the heat-treated glass. In the PG, there are four absorption peaks at 686 nm, 794 nm, 1210 nm, and 1690 nm corresponding to the energy level transitions of Tm^{3+} ions from the ground state to $^3F_2$, $^3H_4$, $^3H_5$, and $^3F_4$ excited states, respectively. After heat

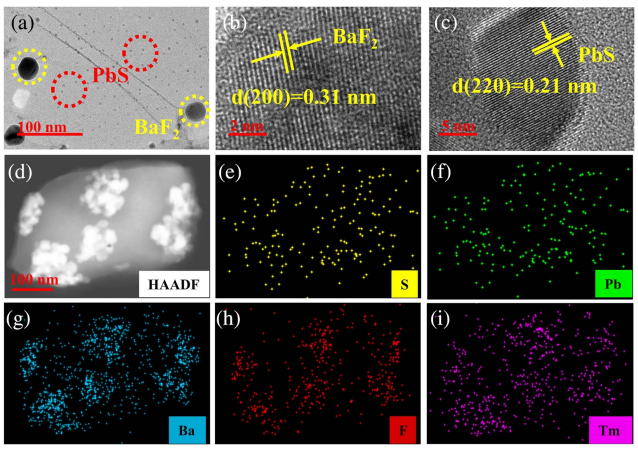

Fig. 3. (a) TEM image and (b), (c) HRTEM images of the glass heat treated at 470°C for 10 h. (d) HAADF-STEM image and (e)–(i) the distribution of representative S, Pb, Ba, F, and Tm elements by two-dimensional element mapping of the glass heat treated at 470°C for 10 h.

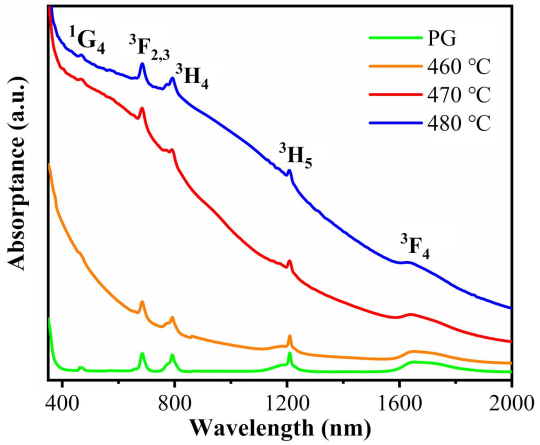

Fig. 4. Absorption spectra of PG and glasses heat treated at different temperatures for 10 h.

treatment, the glasses have a wider absorption band in the NIR range, especially the glass heat treated at 470°C, which is related to the formation of PbS QDs. As the heat treatment temperature increases, BaF_2 NCs and PbS QDs are gradually precipitated in the glass, the color of the glasses becomes darker, and the absorption rate gradually increases.

To explore the luminescent performance of the glass samples, an 808 nm laser was used as the excitation source to measure the NIR emission [Fig. 5(a)]. The emission at 1810 nm is obtained in the PG, which is ascribed to the emission of electrons in the $3F_4$ energy state of the Tm^{3+} metastable state and reaching the ground state $3F_6$. In the heat-treated glass, the emission peak at 1810 nm also appears, which has a significant emission enhancement compared with the PG. This is due to the precipitation of BaF_2 NCs in the glass, which provides a crystal field with lower phonon energy for Tm^{3+} ions. At the same time, another broadband emission peak can be observed, and, as the heat treatment temperature increases, its emission peak position moves from 1200 nm to 2000 nm. Since the emission peak position of Tm^{3+} ions is fixed and located at 1810 nm, it can be inferred that the tunable emission originates from the emission of PbS QDs. Due to the quantum confinement effect, as the heat treatment temperature increases, the size of the PbS QDs increases, and the bandgap structure becomes smaller. Thus, the corresponding PL spectrum will be red-shifted. When the glass is heat treated at 470°C, the emission of PbS QDs and Tm^{3+} ions can combine as an ultra-broadband NIR emission covering 1200–2000 nm with FWHM over 430 nm [Fig. 5(b)]. To further discuss the luminescence mechanism of the glass samples, the fluorescence lifetime was explored, as shown in Fig. 5(c). It can be observed that as the heat treatment temperature increases, the luminescence gradually increases, and the fluorescence lifetime at 1810 nm increases from 0.678 ms to 1.082 ms. Since Tm^{3+} ions are mainly confined in the BaF_2 NCs, which means that the distance between Tm^{3+} ions and PbS QDs is larger than that for energy transfer, it is difficult to transfer energy from PbS QDs to Tm^{3+} ions. Power-dependent photoluminescence (PL) spectra of the glass heat treated at 470°C are shown in Fig. 5(d). It can be observed that the emission of Tm^{3+} ions at 1810 nm increases with the increase of laser power. When the laser power reaches 2.1 W, the emission intensity from PbS QDs reaches saturation relative to that from Tm^{3+} ions. With further increase of power, the intensity of PL is relatively reduced, which is due to the thermal quenching of PL intensity.

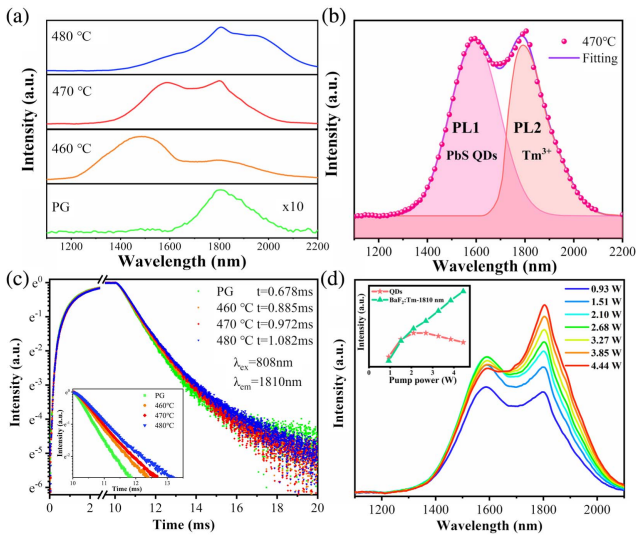

Fig. 5. (a) PL spectra of PG and glasses heat treated at different temperatures for 10 h excited by an 808 nm laser. (b) PL spectra of the glass heat treated at 470°C; PL1 and PL2 are the luminescence bands related to the PbS QDs and Tm^{3+} ions. (c) Lifetime decay curves of the glass samples. The inset is the enlarged curves. The excitation wavelength is 808 nm, and the emission wavelength is 1810 nm. (d) Power-dependent PL spectra of the glass heat treated at 470°C. The inset is PL intensity of the luminescence bands related to the PbS QDs and Tm^{3+} ions.

In practical applications, the influence of ambient temperature on the luminescence of PbS QDs and BaF_2 : Tm^{3+} NCs is of great significance to the design of devices. In Fig. 6, we further explore the temperature-dependent emission of the glass. As the test temperature increases, the luminescence peak of PbS QDs gradually shifts to a longer wavelength [Fig. 6(b)]. There are two main reasons for this phenomenon: electron-phonon coupling and thermal expansion of crystals[29]. At the same time, it is observed that the emission intensity of PbS QDs and Tm^{3+} ions gradually decreases with the increase of temperature, which is a typical thermal-quenching process. As the temperature increases, the vibration energy of the host lattice increases, and the non-radiative process is enhanced, which leads to the loss of luminescence. But PbS QDs and Tm^{3+} ions show different downward trends with the increasing temperature. Therefore, we can use their emission intensity ratio for temperature detection. Figure 6(c) shows that the fluorescence intensity ratio (FIR) emitted by Tm^{3+} ions to PbS QDs has an exponential relationship with temperature. The expression is as follows, and the correlation coefficient is as high as 99.5%[30]:

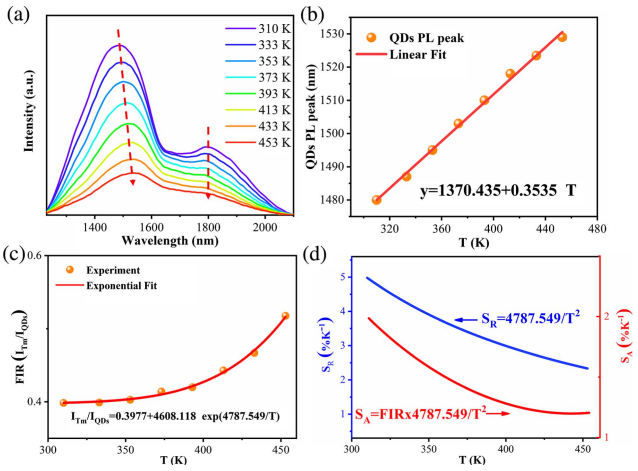

Fig. 6. (a) Temperature-dependent PL spectra of glass heat treated at 460°C. (b) Temperature dependence of the PbS QDs PL peak position. (c) The FIR of I_{Tm}/I_{QDs} as a function of temperature in the range of 310–453 K. (d) The relative sensitivity S_R and the absolute sensitivity S_A in (c).

$$\mathrm{FIR}(I_{\mathrm{Tm}}/I_{\mathrm{QDs}}) = A + B\exp\left(-\frac{\Delta E}{k_B T}\right). \tag{2}$$

In the above formula, A, B are constants, ΔE is the thermal-quenching energy level difference of the non-thermal coupling system, k_B is the Boltzmann constant, and T is the absolute temperature.

To further measure its absolute temperature performance, it is necessary to evaluate the absolute sensitivity S_A and relative sensitivity S_R, and the expression is as follows:

$$S_A = \frac{\mathrm{d(FIR)}}{\mathrm{d}T} = \mathrm{FIR} \times \frac{\Delta E}{k_B T^2}, \tag{3}$$

$$S_R = \frac{1}{\mathrm{FIR}}\frac{\mathrm{d(FIR)}}{\mathrm{d}T} = \frac{\Delta E}{k_B T^2}. \tag{4}$$

As shown in Fig. 6(d), it can be seen that in the temperature range of 310–453 K, both S_R and S_A decrease monotonously with increasing temperature. In addition, the relative sensitivity and absolute sensitivity of FIR reach the maximum values of 4.98% and 1.99% at 310 K. The above results show that it also has a good application prospect in the field of optical thermometry.

4. Conclusions

PbS QDs and BaF_2 NCs-doped glasses were fabricated by the melt-quenching method and subsequent heat treatment. According to the XRD and TEM test results, PbS QDs and BaF_2 NCs were uniformly precipitated in the glass. With the heat treatment temperature increased from 460°C to 480°C, the sizes of PbS QDs and BaF_2 NCs increased obviously. Under the excitation of 808 nm LD, the $Tm^{3+}: {}^3F_4 \rightarrow {}^3H_6$ emission at 1810 nm and the NIR tunable emission of PbS QDs appeared in the heat-treated glass simultaneously. When the emissions of PbS QDs and Tm^{3+} ions overlap after proper heat treatment, ultra-broadband emission in the NIR regions can be obtained, the emission range is 1200–2000 nm, and the FWHM reaches 430 nm, which shows great potential in the field of broadband fiber amplifiers.

Acknowledgement

This work was financially supported by the Key R&D Program of Guangzhou (No. 202007020003), National Natural Science Foundation of China (Nos. 62122027, 52002128, 62075063, 51772101, and 51872095), China Postdoctoral Science Foundation (Nos. 2020M672621 and 2021M691054), Local Innovative and Research Teams Project of Guangdong Pearl River Talents Program (No. 2017BT01X137), and State Key Laboratory of Advanced Technology for Materials Synthesis and Processing, Wuhan University of Technology (No. 2020-KF-19).

References

1. Y. Wang, N. K. Thipparapu, D. J. Richardson, and J. K. Sahu, "Ultra-broadband bismuth-doped fiber amplifier covering a 115-nm bandwidth in the O and E bands," J. Lightwave Technol. **39**, 795 (2021).
2. A. W. Naji, B. A. Hamida, X. S. Cheng, M. A. Mahdi, S. Harun, S. Khan, W. F. Al-Khateeb, A. A. Zaidan, B. B. Zaidan, and H. Ahmad, "Review of erbium-doped fiber amplifier," Int. J. Phys. Sci. **6**, 4674 (2011).
3. N. K. Thipparapu, Y. Wang, S. Wang, A. A. Umnikov, P. Barua, and J. K. Sahu, "Bi-doped fiber amplifiers and lasers," Opt. Mater. Express **9**, 2446 (2019).
4. Z. Hu, Z. Liu, Z. Zhan, T. Shi, J. Du, X. Tang, and Y. Leng, "Advances in metal halide perovskite lasers: synthetic strategies, morphology control, and lasing emission," Adv. Photonics **3**, 034002 (2021).
5. S. Zhang, D. Li, and G. Zhao, "Tunable all-fiber Er^{3+}-doped laser based on a double-clad Er^{3+}/Yb^{3+} co-doped fiber amplifier," Microw. Opt. Technol. Lett. **50**, 2671 (2008).
6. L. Guo, S. Zhao, T. Li, W. Qiao, B. Ma, Y. Yang, K. Yang, H. Nie, B. Zhang, R. Wang, J. He, and Y. Wang, "In-band pumped, high-efficiency LGS electro-optically Q-switched 2118 nm Ho:YAP laser with low driving voltage," Opt. Laser Technol. **126**, 106015 (2020).
7. Y. Zhao, D. Zhao, R. Liu, W. Ma, and T. Wang, "Switchable generation of a sub-200 fs dissipative soliton and a noise-like pulse in a normal-dispersion Tm-doped mode-locked fiber laser," Appl. Opt. **59**, 3575 (2020).
8. Y. Xie, Z. Liu, Z. Cong, Z. Qin, S. Wang, Z. Jia, C. Li, G. Qin, X. Gao, and X. Zhang, "All-fiber-integrated Yb:YAG-derived silica fiber laser generating 6 W output power," Opt. Express **27**, 3791 (2019).
9. Y. Wang, J. Wu, Q. Zhao, W. Wang, J. Zhang, Z. Yang, S. Xu, and M. Peng, "Single-frequency DBR Nd-doped fiber laser at 1120 nm with a narrow linewidth and low threshold," Opt. Lett. **45**, 2263 (2020).
10. C. Jiang, "Modeling and gain properties of Er^{3+} and Pr^{3+} codoped fiber amplifier for 1.3 and 1.5 μm windows," J. Opt. Soc. Am. B **26**, 1049 (2009).
11. X. Shen, Y. Zhang, L. Xia, J. Li, G. Yang, and Y. Zhou, "Dual super-broadband NIR emissions in Pr^{3+}-Er^{3+}-Nd^{3+} tri-doped tellurite glass," Ceram. Int. **46**, 14284 (2020).
12. J. Liu, X. Huang, H. Pan, X. Zhang, X. Fang, W. Li, H. Zhang, A. Huang, and Z. Xiao, "Broadband near infrared emission of Er^{3+}/Yb^{3+} co-doped fluoro-tellurite glass," J. Alloys Compd. **866**, 158568 (2021).
13. M. Zhang, W. Zheng, Y. Liu, P. Huang, Z. Gong, J. Wei, Y. Gao, S. Zhou, X. Li, and X. Chen, "A new class of blue-LED-excitable NIR-II luminescent nanoprobes based on lanthanide-doped CaS nanoparticles," Angew. Chem. Int. Ed. **58**, 9556 (2019).
14. S. Wen, J. Zhou, K. Zheng, A. Bednarkiewicz, X. Liu, and D. Jin, "Advances in highly doped upconversion nanoparticles," Nat. Commun. **9**, 2415 (2018).

15. L. Cormier and S. Zhou, "Transition metals as optically active dopants in glass-ceramics," Appl. Phys. Lett. **116**, 260503 (2020).
16. J. Ren, X. Lu, C. Lin, and R. K. Jain, "Luminescent ion-doped transparent glass ceramics for mid-infrared light sources," Opt. Express **28**, 21522 (2020).
17. C. Lin, L. Li, S. Dai, C. Liu, Z. Zhao, C. Bocker, and C. Rüssel, "Oxyfluoride glass-ceramics for transition metal ion based photonics: broadband near-IR luminescence of nickel ion dopant and nanocrystallization mechanism," J. Phys. Chem. C **120**, 4556 (2016).
18. J. Xue, X. Wang, J. H. Jeong, and X. Yan, "Fabrication, photoluminescence and applications of quantum dots embedded glass ceramics," Chem. Eng. J. **383**, 123082 (2020).
19. F. P. Garcia de Arquer, D. V. Talapin, V. I. Klimov, Y. Arakawa, M. Bayer, and E. H. Sargent, "Semiconductor quantum dots: technological progress and future challenges," Science **373**, 6555 (2021).
20. X. Huang, Q. Guo, D. Yang, X. Xiao, X. Liu, Z. Xia, F. Fan, J. Qiu, and G. Dong, "Reversible 3D laser printing of perovskite quantum dots inside a transparent medium," Nat. Photon. **14**, 82 (2020).
21. Z. Cao, F. Hu, C. Zhang, S. Zhu, M. Xiao, and X. Wang, "Optical studies of semiconductor perovskite nanocrystals for classical optoelectronic applications and quantum information technologies: a review," Adv. Photonics **2**, 054001 (2020).
22. G. Dong, H. Wang, G. Chen, Q. Pan, and J. Qiu, "Quantum dot-doped glasses and fibers: fabrication and optical properties," Front. Mater. **2**, 13 (2015).
23. X. Huang, Z. Fang, S. Kang, W. Peng, G. Dong, B. Zhou, Z. Ma, S. Zhou, and J. Qiu, "Controllable fabrication of novel all solid-state PbS quantum dot-doped glass fibers with tunable broadband near-infrared emission," J. Mater. Chem. C **5**, 7927 (2017).
24. R. Martin-Rodriguez, R. Geitenbeek, and A. Meijerink, "Incorporation and luminescence of Yb^{3+} in CdSe nanocrystals," J. Am. Chem. Soc. **135**, 13668 (2013).
25. E. O. Serqueira and N. O. Dantas, "Determination of the energy transfer section between CdS semiconductor quantum dots and Nd ions," Opt. Mater. **90**, 252 (2019).
26. Z. Peng, X. Huang, Z. Ma, G. Dong, and J. Qiu, "Surface modification and fabrication of white-light-emitting Tm^{3+}/CdS quantum dots co-doped glass fibers," J. Am. Ceram. Soc. **102**, 5818 (2019).
27. G. Kresse and D. Joubert, "From ultrasoft pseudopotentials to the projector augmented-wave method," Phys. Rev. B **59**, 1758 (1999).
28. G. Kresse and J. Furthmuller, "Efficiency of ab-initio total energy calculations for metals and semiconductors using a plane-wave basis set," Comput. Mater. Sci. **6**, 15 (1996).
29. X. Huang, Z. Peng, Q. Guo, X. Song, J. Qiu, and G. Dong, "Energy transfer process and temperature-dependent photoluminescence of PbS quantum dot-doped glasses," J. Am. Ceram. Soc. **102**, 3391 (2019).
30. S. A. Wade, S. F. Collins, and G. W. Baxter, "Fluorescence intensity ratio technique for optical fiber point temperature sensing," J. Appl. Phys. **94**, 4743 (2003).